Inhibitors of Kinesin Activity from Structure-Based Computer Screening†

Seth C. Hopkins,*,‡,⊥ Ronald D. Vale,§,∥ and Irwin D. Kuntz‡

Department of Pharmaceutical Chemistry, Howard Hughes Medical Institute, and Department of Cellular and Molecular Pharmacology, University of California, San Francisco, California 94143-0446

Received October 25, 1999

ABSTRACT: Kinesin motor proteins use ATP hydrolysis for transport along microtubules in the cell. We sought to identify small organic ligands to inhibit kinesin's activity. Candidate molecules were identified by computational docking of commercially available compounds using the computer program DOCK. Compounds were docked at either of two sites, and a selection was tested for inhibition of microtubule-stimulated ATPase activity. Twenty-two submillimolar inhibitors were identified. Several inhibitors appeared to be competitive for microtubule binding and not for ATP binding, and three compounds showed 50% inhibition down to single-digit micromolar levels. Most inhibitors grouped into four distinct classes (fluoresceins, phenolphthaleins, anthraquinones, and naphthylene sulfonates). We measured the binding of one inhibitor, rose bengal lactone (RBL), to kinesin (dissociation constant 2.5 μM) by its increase in steady-state fluorescence anisotropy. The RBL binding site on kinesin was localized by fluorescent resonance energy transfer (FRET) using a donor fluorophore (coumarin) covalently attached at unique, surface-exposed cysteine residues engineered at positions 28, 149, 103, 220, or 330. RBL was found to bind in its original docked site: the pocket cradled by loop 8 and β-strand 5 in kinesin's three-dimensional structure. These results confirm this region's role in microtubule binding and identify this pocket as a novel binding site for kinesin inhibition.

Members of the kinesin superfamily are responsible for a variety of intracellular microtubule-based transport functions, including organelle transport, chromosome movement during mitosis and meiosis, maintenance of endoplasmic reticulum and intermediate filament distributions, as well as spindle formation, flagellar growth, and positioning of developmental morphogens (*1*). The family of conventional kinesins, involved in organelle transport, is composed of an N-terminal motor domain, a coiled-coil region that maintains a dimerized form, and a C-terminal tail region that binds to the macromolecular target or cargo to be transported. Crystal structures of the motor domains (∼350 aa) have been solved for conventional kinesins (*2*−*4*), as well as for members of another kinesin family distinguished by its C-terminal motor domain (*5*−*7*). The three-dimensional structure of kinesin's motor domain shows similarities to the actin-based myosin motor (*2, 8*) as well as to G-proteins (*9*), suggesting that these protein superfamilies may have arisen through divergent evolution from a common ancestor (*10*).

An inhibitor for kinesin could prove useful to probe its mechanism and its function in vivo. The development of kinesin inhibitors may ultimately have clinical utility, much in the way that compounds that interfere with tubulin polymerization are effective against cancer by causing mitotic arrest (*11, 12*). Aside from nucleotide analogues, no drugs are known to target kinesins, and there is only one reported nonnucleotide kinesin inhibitor (*13*). This inhibitor, adocia-sulfate-2 (AS-2), a natural product of marine sponges, is difficult to purify and currently is not synthesized. AS-2 inhibits kinesin's microtubule-stimulated ATP hydrolysis with a median inhibitory concentration in the low micromolar range by competing with microtubules for binding to kinesin. Unfortunately, there is no structural information about the binding site of AS-2, and a structural mechanism for its competition with microtubules is not known, limiting the development of related inhibitors.

In this paper we used a structure-based approach to screen for kinesin ligands. This consisted of computationally screening potential ligands using the computer program DOCK, followed by biochemically screening for inhibitors of ATPase activity. Previously, this approach has identified inhibitors to a variety of protein systems, including inhibitors of HIV-1 protease (*14*), thymidylate synthase (*15*), influenza hemagglutinin (*16*), and purine salvage enzymes in parasitic protozoa (*17*). DOCK provides a rapid method for identifying inhibitors among commercially available compounds. Specificity and affinity can then be improved using structural information from the inhibitor's binding mode in a cycle of structure-based design (*18*). To initiate this cycle, we identified several classes of submillimolar kinesin inhibitors. We chose one compound for structural characterization and found that it bound in our original docking site. Structure-based ligand design efforts can now be focused at this novel binding site for more selective and tighter binding kinesin inhibitors.

† This work was supported by a grant from the National Institute of General Medical Sciences (GM 31497 to I.D.K.) and the National Institutes of Health (PO1 AR42895 to R.D.V).

* Address correspondence to this author. Telephone: (415) 476-5326. Fax: (415) 502-1411. E-mail: seth@itsa.ucsf.edu.

‡ Department of Pharmaceutical Chemistry.

§ Howard Hughes Medical Institute.

∥ Department of Cellular and Molecular Pharmacology.

⊥ Current address: Sepracor, 111 Locke Dr., Marlborough, MA 01752.

10.1021/bi992474k CCC: $19.00
Published on Web 02/18/2000

METHODS

Computations. DOCK 4.0 (*19*−*21*) was used to screen the ACD[1] (versions 95.1 and 97, Molecular Design Limited Information Systems, San Leandro, CA) for potential kinesin inhibitors. Each compound's rigid conformation, as generated by CONCORD (*22*, *23*), was docked in turn to kinesin. All crystallographic waters, ADP, ions, and solvent were removed from the crystal structure of human conventional kinesin as solved by Kull and co-workers (*2*). The computer program SPHGEN (*19*) was used to create clusters of overlapping spheres in contact with kinesin's solvent-accessible surface, from which two suitable binding sites on kinesin were selected. The sphere positions in the dock sites were selected using interactive graphical display of the surface curvature and electrostatic surface potentials calculated by Grasp (*24*). At each binding site, the sphere cluster was used to create a negative image of the docking site. DOCK matched each compound in turn to the site's negative image to search for favorable binding orientations. DOCK scored each orientation based on the ligand's complementarity to the protein surface using an interaction force field score that included van der Waals and electrostatic terms (*20*). To assist the selection of potential ligands, the docked orientations were also evaluated with a scoring scheme based on the ligand surface area in contact with kinesin's surface. Subsets of the ACD were created using the filtering programs UCSelect (*25*) and Merlin (*26*) with the intention of removing compounds with undesirable molecular weights, ClogP values (an estimate of hydrophobicity based on a calculated logarithm of the octanol−water partitioning), and reactive functional groups. This reduced the ACD from ∼200 000 compounds to ∼110 000 compounds. Of these, the highest-scoring 500−1000 compound-bound orientations were output by DOCK. These compounds were clustered based on measures of their structural similarities, using Daylight's Merlin system (*26*) of hashed connectivity fingerprints, and according to a complete linkage hierarchical clustering algorithm. A minimum intracluster Tanimoto similarity metric of 0.85 was used, and only the top-scoring compounds from each cluster were considered further. Compounds were selected for testing based on graphical inspection of each ligand's binding mode using MidasPlus 2.1 (*27*, *28*) and Sybyl 6.5 (*29*). Compounds that inhibited kinesin in the assays were used as seeds in new fingerprint searches for additional compounds from the ACD with common substructures, and these groups of similar compounds were also docked. All docking was performed on an R10000 197 MHz processor (SGI, Mountain View, CA).

Chemicals. All chemicals used in the screening were purchased from Sigma Chemical, Aldrich, the Sigma−Aldrich Library of Rare Chemicals (SALOR), Maybridge (Ryan Scientific, SC), or Acros Organics. Fluorophores for FRET experiments were purchased from Molecular Probes (Eugene, OR). Pyruvate kinase, lactate dehydrogenase, and AMP-PNP were purchased from Boehringer Mannheim (Boehringer Mannheim, Indianapolis, IN).

Kinesin. All compounds purchased were screened for inhibition of human ubiquitous kinesin (K560) ATPase. K560 was expressed as a bacterial recombinant protein of amino acids 1−560 with a C-terminal six-histidine tag in the *Nde*I/*Xho*I site of the IPTG-inducible pET17b plasmid (Novagen, Inc.). Bacterial cells were harvested, lysed, and purified on a Ni-NTA column (Qiagen, Inc.) followed by a 25 mL DEAE-Sepharose fast-flow column and fractionated with a NaCl gradient (0.05−1 M). Fractions containing K560 were pooled, made 10% w/v in sucrose, and stored in liquid nitrogen. Alternatively, a human kinesin with all but one surface-exposed cysteine residue (cysteine light mutant K349 kinesin, CLM) mutated to either serine or alanine was expressed as a bacterial recombinant protein of amino acids 1−349 resulting in monomeric constructs with single cysteines at the following positions: 330 (CLM-C330), 220 (CLM-C220), 149 (CLM-C149), 103 (CLM-C103), or 28 (CLM-C28). Bacterial cells were harvested, lysed, and purified on a phosphocellulose column (Whatman, Farifield, NJ), and fractionated with a KCl gradient (0.01−0.1 M). Peak fractions were pooled, diluted to 0.01 M KCl, and loaded onto a Resouce S column (Amersham Pharmacia Biotech, Piscataway, NJ), and the flow-through was collected. The flow-through was dialyzed to increase its pH to 8.0 and further fractionated over a Resource Q column (Amersham Pharmacia Biotech, Piscataway, NJ) with a 0.003−0.040 M KCl gradient. Fractions containing CLM were pooled, made 10% w/v sucrose, and stored in liquid nitrogen.

Protein Labeling. Single surface-exposed cysteine CLM kinesin was exchanged into labeling buffer (25 mM Pipes, pH 7.0, 50 mM NaCl, 2 mM $MgCl_2$, 1 mM EGTA, 0.02% Tween-20, 10 μM ATP, and 0.1 M TCEP) by multiple centrifugations using a Centricon concentrator (Amicon, Inc., Beverly, MA). A 5−10-fold excess of 7-diethylamino-3-(4′-maleimidylphenyl)-4-methylcoumarin dye (CPM, Molecular Probes #D-346, Eugene, OR) was added, and the reaction was left at room temperature for 3 h. The excess dye was removed by multiple centrifugations through a Centricon concentrator. The stoichiometry of binding was measured by the dye's absorbance and a Bradford assay of protein concentration using a BSA standard.

Motility Assays. Kinesin (K560) motility was measured in vitro with an epifluorescence microscope. Fluorescent rhodamine-labeled microtubules (*30*) were observed to glide over a kinesin-coated coverslip in the presence of an oxygen depletion system (71.5 mM β-mercaptoethanol, 22.5 mM glucose, 0.22 mg/mL glucose oxidase, 0.036 mg/mL catalase). A 10 μL reaction containing BRB80 (80 mM Pipes, pH 6.8, 1 mM EGTA, and 1 mM $MgCl_2$), 2.5 mg/mL casein, 1 mM ATP, compound, and microtubules was injected into a flow-chamber constructed by placing a coverslip across two pieces of double-stick tape on a microscope slide. The amount of kinesin added to the 10 μL reaction was decreased (by diluting with 0.5 mg/mL casein in BRB80) until no microtubules were observed to bind within 3 min. This typically occurred around 0.2 μg/mL kinesin. The assay then was performed at a kinesin level ∼10-fold more than this threshold. In the case of fluorescent and highly colored compounds, differential interference optics were used in place of the epifluorescence to image the microtubules.

[1] Abbreviations: ACD, Available Chemicals Directory; Pipes, piperazine-*N*,*N*′-bis(2-ethanesulfonic acid); EGTA, ethylene glycol bis-(aminoethyl ether)-*N*,*N*,*N*′,*N*′-tetraacetic acid; NADH, β-nicotinamide adenine dinucleotide, reduced form; FRET, fluorescence resonance energy transfer; RBL, rose bengal lactone.

Assays of ATPase. Microtubule-stimulated ATPase was assayed using a malachite green phosphate assay (*31*). Tubulin was purified as in ref *30*, and microtubules were polymerized from frozen aliquots of tubulin before each week of assays, as described previously (*32*). To screen for inhibitors, assays were performed in 100 μL reactions at room temperature containing 1.2 μM microtubules, 20 μM paclitaxel, 1 mM ATP, and buffer BRB12 (12 mM Pipes, pH 6.8, 1 mM EGTA, and 1 mM $MgCl_2$). The ATPase reaction was initiated by addition of 1 μL of 0.02 mg/mL K560, and 10 μL aliquots were taken over 30 min to monitor phosphate concentration. Stock solutions of inhibitors were made 100 mM in dimethyl sulfoxide (DMSO) and stored at room temperature in the dark. To screen for inhibition at 1 mM, 1 μL of stock was diluted to 10 μL with DMSO (to aid compound solubility), and this was added to the 100 μL reactions. Each set of measurements contained four compound reactions and a 10% DMSO control for a total of five parallel reactions. ATP hydrolysis was expressed as a percent of this control rate. An alternate method of measuring ATPase used a coupled-enzyme system of pyruvate kinase (PK) and lactate dehydrogenase (LDH) which regenerates ATP from ADP (*33*). About 8 μg/mL kinesin was added to a reaction of 100 μL containing the compound to be tested with 40 μg/mL PK, 100 μg/mL LDH, 250 μM NADH, 2.5 mM phosphoenol pyruvate, in BRB12, and total DMSO at 1%. The pyruvate kinase regenerates ATP from ADP, and lactate dehydrogenase oxidizes NADH stoichiometrically with pyruvate as the intermediate. This oxidation of NADH is monitored spectrophotometrically at 340 nm. Many of the compounds also absorbed at this wavelength, so this assay was not used for compounds whose 50% inhibitory concentration of kinesin was greater than 50 μM. To ensure that the compounds were not inhibiting the coupled enzyme system at the levels of added enzyme used in the assays, 1 mM ADP was added in control runs, in the presence and absence of compound, and the maximal rate of ATP regeneration was measured.

IC_{50} Intervals. Due to the large number of compounds, estimates of the mean inhibitory concentrations (IC_{50}) are reported as intervals reasonably certain to contain the true IC_{50} value. Serial dilutions of submillimolar inhibitors were performed until inhibition vanished. A compound that inhibited hydrolysis at concentration [B], and whose dilution removed inhibition at concentration [A], had its true IC_{50} value represented as greater than [A] and less than [B]. Below 20% of control, hydrolysis was considered to be inhibited and above 80%, not inhibited. In cases where the hydrolysis was moderately inhibited, between 35% and 65% of control, the true IC_{50} value was expressed as an interval between 1/2 and 2 times the concentration at which this inhibition was measured. The serial dilutions were aimed at rough estimates of the true IC_{50} value, but since the assays were labor-intensive, we accepted the resulting levels of uncertainty. For the better inhibitors, the true IC_{50} values were measured both with the malachite green phosphate assay and with the coupled enzyme ATPase assay.

Microtubule Sedimentation Assays. The binding of kinesin to microtubules was measured by microtubule sedimentation assays. K560 fused to green fluorescent protein (*34*) (K560-GFP) at 0.02 μg/mL was incubated for 3 min with 0.2, 0.5, 1.0, 2.0, 5.0, or 15 μM microtubules in BRB12 containing 5 mM nonhyrolyzable ATP analogue AMP-PNP. The reaction was then centrifuged in a TLA 100.4 Ultracentrifuge (Beckman, Inc.) for 5 min, supernatant was removed, and microtubule pellet was resuspended and depolymerized on ice. The amount of GFP fluorescence in the pellet was quantified in a fluorometer with 488 nm excitation and 512 nm emission.

Fluorescence Spectroscopy. Fluorescence spectra and steady-state anisotropy of RBL were measured with a Xenon lamp fluorometer (SLM Instruments, Inc.) with adjustable monochromators. Anisotropy measurements were made with Glann-Thompson prism polarizers in the excitation and emission light paths, and redundant combinations of polarized intensities were measured to determine the instrumental correction factor for the different instrumental transmission efficiencies of vertically and horizontally polarized light. Binding curves of RBL were measured in 15 μL samples containing 2 μM kinesin in BRB12 and RBL concentrations ranging between 0.167 and 33 μM. At the lower concentrations, 2 s of photon counting was used to measure intensities. The anisotropy of RBL in buffer was independent of concentration over this range. The FRET efficiencies were estimated as $E = 1 - (F_{da}/F_d)$, where F_{da} and F_d are the fluorescence of the donor in the presence and absence of the acceptor, respectively. To determine an accurate value for F_{da}, we fitted the peak fluorescence intensities to the binding equation $y = a[\mathrm{RBL}]/(b + [\mathrm{RBL}]) + c$, where y is the normalized intensity, [RBL] is the total concentration of RBL, and a, b, and c are adjustable parameters. The asymptote of this curve ($a + c$) was taken as the limiting amount of intensity resulting from RBL saturating the donor-labeled kinesin. In cases where the saturating intensities were close to zero, the asymptote became negative, so a value of zero intensity (complete transfer) was used to calculate the transfer efficiency E. The FRET distance R was calculated from Förster's equation: $E = 1/[1 + (R/R_o)^6]$, where R_o (in Å) $= 0.221(Q_D\kappa^2 n^{-4} J)^{1/6}$, n is the refractive index of the medium (assumed to be 1.4), κ^2 is the orientation parameter (assumed to be 2/3) (*35*), Q_D is the donor quantum yield [0.5 for coumarin (*36*)], and J is the donor−acceptor spectral overlap of donor and acceptor [10×10^{14} M^{-1} cm^{-1} nm^4 for coumarin−eosin (*36*)]. We assumed the R_o value for the coumarin−RBL pair to be that of the coumarin−eosin pair (45 Å) based on both the structural and the spectral similarity between eosin and RBL (*36*).

RESULTS

Compound Docking. To disrupt kinesin's function, we considered two binding sites for candidate ligands, one in the active site where ADP was bound, and the other adjacent to the putative microtubule binding region. The two sites for docking were chosen from the clusters of spheres created by SPHGEN (*19*) as described under Methods. The sphere clusters, essentially negative images of a docking site, were used in DOCK to rapidly generate bound configurations of ligand (*21*). Figure 1 shows the cluster of 74 spheres that occupied the active site and included the region where ADP was bound. Using this sphere cluster, a control run of the DOCK parameters used in the screening reproduced the crystallographic configuration of ADP to within 2.6 Å rmsd. A total of 110 000 compounds were rigidly docked at the active site at an average of 11 s per compound. After

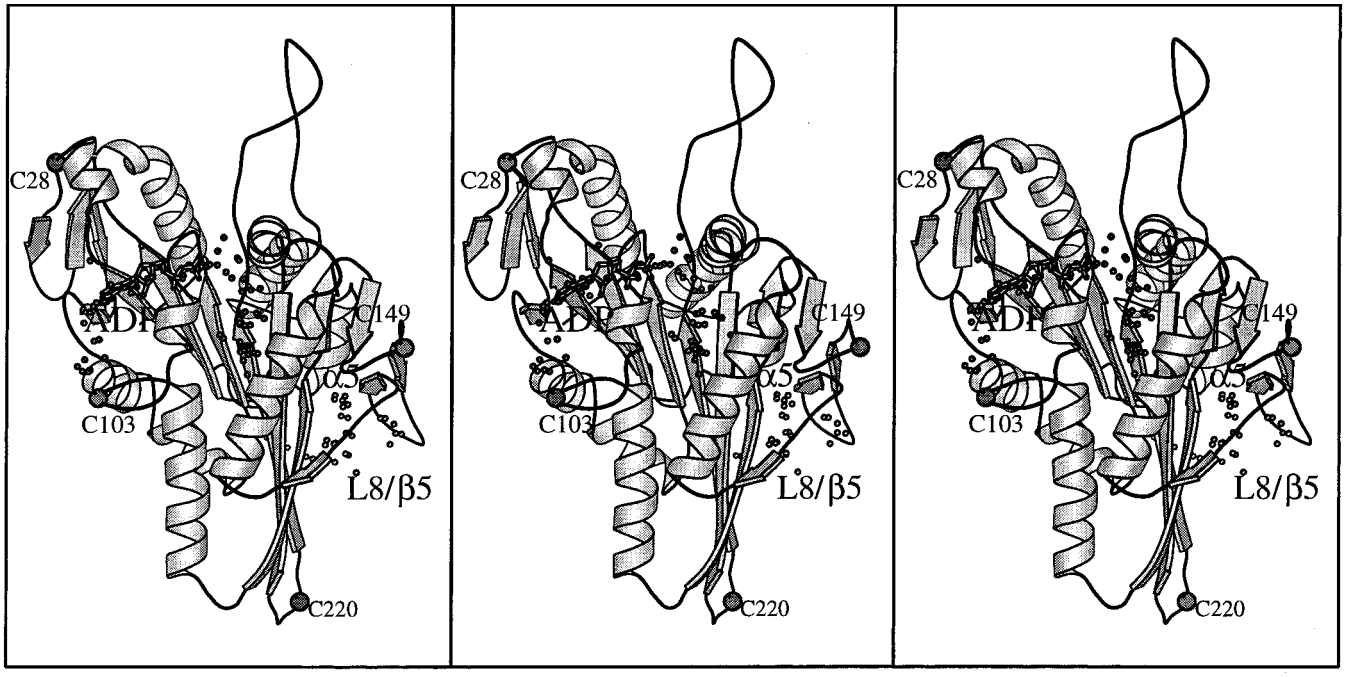

FIGURE 1: Stereo diagram of the two docking sites on kinesin. The clusters of small spheres define the extent of each site and are used in DOCK to generate bound ligand orientations. The active site is shown with a bound ADP. The L8/β5 site is adjacent to kinesin's putative microtubule binding face. Cross-eyed view, left two images; wide-eyed view, right two images. Protein Data Bank code: 1bg2 (*2*). For later reference, the positions of cysteine mutations for FRET experiments are displayed here. The tip of the extensive loop in the upper part of the structure was not resolved in the crystal structure (*2*). Figure made with MolScript (*50*).

clustering and graphical inspection, 37 compounds from this run were tested for inhibition of ATPase.

In an attempt to interfere with microtubule binding, we chose a second docking site near important microtubule binding residues as identified by alanine-scanning mutagenesis (*32*) and by proteolytic digests (*37*). A cluster of 33 spheres occupied a fairly recessed region on the kinesin surface, defining a positively charged pocket on a relatively negatively charged face of the protein. The location of this docking site, referred to as the L8/β5 dock site, is shown in Figure 1. A total of 115 400 uncharged compounds were rigidly docked in the L8/β5 dock site at an average of 19 s per compound. After clustering and graphical evaluation, a total of 28 compounds from this run were tested for inhibition of ATPase. Thus, a combined total of 65 compounds were tested from both dock runs.

Inhibition of ATPase. All 65 compounds suggested by these 2 dock runs were screened at 1 mM for inhibition of K560 ATPase. The microtubule concentration was kept at $\sim$1.2 μM, where hydrolysis rates were approximately half-maximal, to ensure the detection of any competition between compound and microtubules. Nine compounds inhibited hydrolysis by 90% or more (9 hits). In a separate screen, all 65 compounds were also tested for inhibition under assay conditions where limiting ATP concentrations (40 μM) produced half-maximal hydrolysis rates in the presence of excess microtubules (15 μM). No new inhibitors were discovered in this ATP-limiting screen (data not shown) that were not already apparent from the microtubule-limiting screen, indicating that none of the 65 compounds competed for ATP binding. This result suggested that despite having docked 37 compounds at the active site, none of these compounds were binding there. Hits in both screens were compounds 267009, 267154, 195710, and RBL; hits from

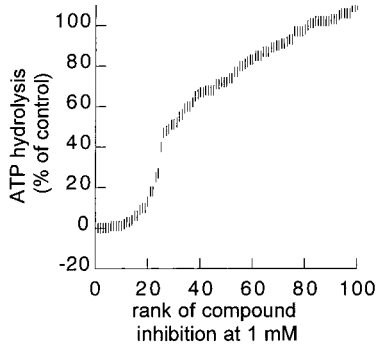

FIGURE 2: Rates of K560 ATPase for each of 102 compounds tested. Rates are expressed as a percent of a DMSO control (see Methods). The maximal hydrolysis rate was limited by the amount of microtubules (1.2 μM tubulin) in the assay.

the microtubule-limited screen, but not apparent in the ATP-limited screen, were compounds 19164, 230702, 128813, 17488, and 133145. Thus, we discovered 9 submillimolar inhibitors out of the 65 compounds suggested by computational screening.

We found 13 more submillimolar inhibitors by searching the ACD for compounds structurally similar to these 9 hits, and docking these to each of the 2 sites in turn. Similarity searches were performed using Daylight's connectivity fingerprints (see Methods) to find groups of compounds with a common substructure. The ATPase rates from the combined total of 102 compounds (both the original docked compounds and those selected after similarity searches) are shown in Figure 2. The majority of the submillimolar inhibitors were grouped into the four classes shown in Figure 3. The inhibitors in the first class all contain a fluorescein substructure (Figure 3, first column). There are over 250 compounds in the ACD that contain a fluorescein core, and of the 6 chosen, all but 1 were submillimolar inhibitors, with

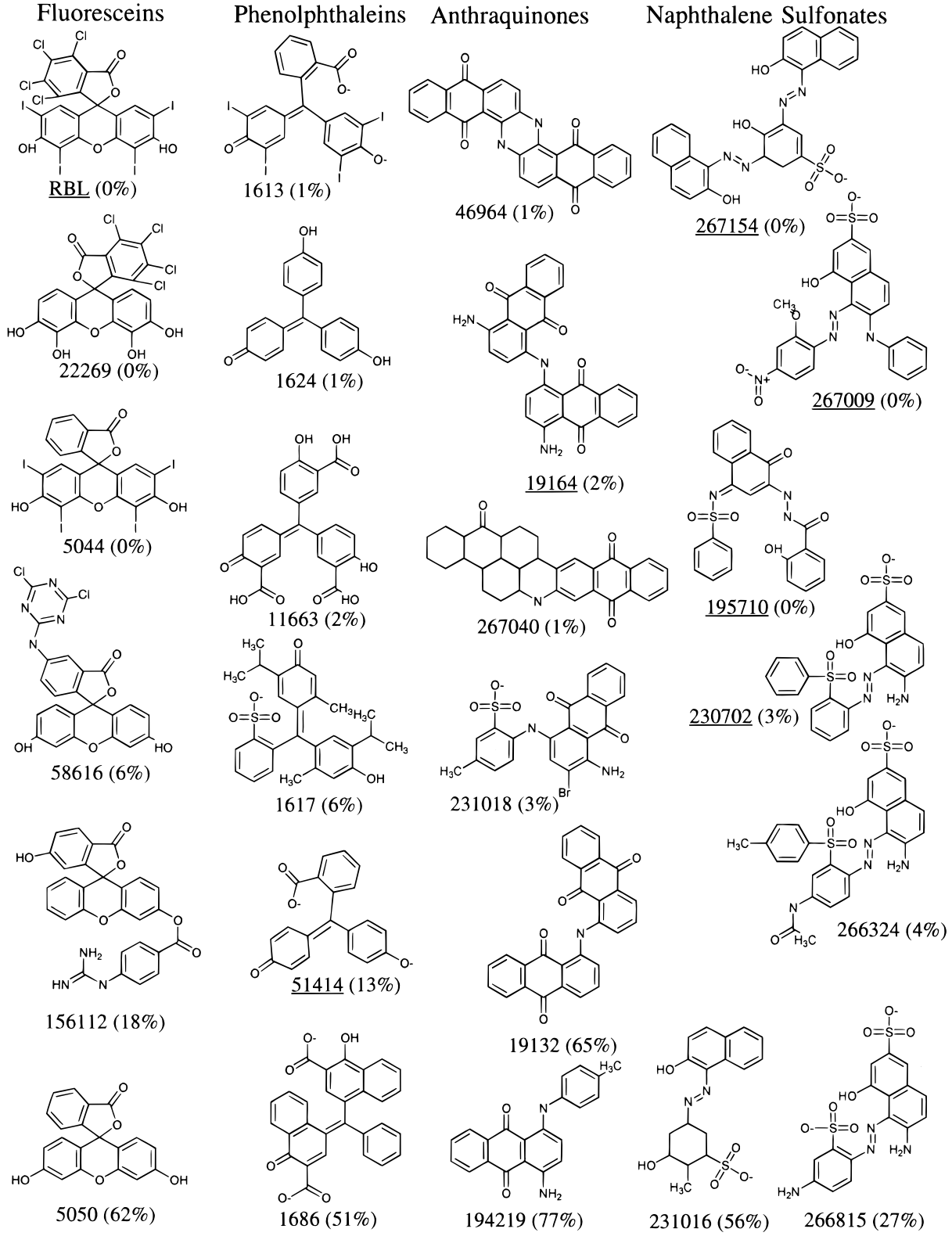

FIGURE 3: Four classes of kinesin inhibitors defined by common substructures. Compounds with underlined names were found by the initial docking screen, and their relatives were found after similarity searches and further docking. The number in parentheses is the percent of control hydrolysis at 1 mM. Compounds were named according to their ACD number, with the exception of RBL.

fluorescein itself (compound 5050 in Figure 3) being the one exception. In a second class of compounds, permutations on a phenolphthalein core were all submillimolar inhibitors except for compound 1686. A third class of inhibitors contained an anthraquinone core, and all were submillimolar inhibitors except for compounds 19132 and 194219. In the class of naphthalein- and sulfonate-containing compounds, only one inhibitor (compound 266324) was discovered through similarity searches. The remaining four inhibitors were selected due to their uniquely high DOCK scores by both force field and contact scoring. In summary, the initial DOCK screening was aimed at rapidly selecting a structurally diverse set of candidate ligands from a large database, and the subsequent similarity searches were aimed at amplifying

Table 1: IC_{50} Intervals (μM) of Kinesin Inhibitors[a]

compounds	K560-M[b]	ncd-MT[c]	unc104-MT[d]	K560−BAS[e]	ncd-BAS	myosin II[f]	motility[g]
fluoresceins							
RBL	7.5 ± 2.5	1.5 ± 0.5	1.8 ± 0.8	<40**	5.3 ± 4.8	25 ± 15	no MT binding
22269	12.5 ± 7.5	30 ± 20	5.0 ± 5.0	>50	125 ± 75	−	−
156112	25 ± 25	55 ± 45	63 ± 38	−	−	−	−
5044	63 ± 38	55 ± 45	25 ± 25	−	50 ± 50	−	−
58616	625 ± 375	625 ± 375	250 ± 250	−	−	−	−
phenylthaleins							
11663	1.4 ± 1.1	0.8 ± 0.3	0.5 ± 0.5	**	>50	50 ± 50	no MT binding
1613	30 ± 20	150 ± 50	25 ± 25	>50	−	1250 ± 750	no MT binding
51414	125 ± 75	150 ± 50	>100	>1000	−	−	−
1617	300 ± 200	75 ± 25	50 ± 50	−	−	−	no MT binding
1624	300 ± 200	55 ± 45	>100	−	−	550 ± 450	normal
anthraquinones							
46964	12.5 ± 7.5	2.5 ± 2.5	5 ± 5	−	−	550 ± 450	no MT binding
19164	125 ± 75	62.5 ± 37.5	25 ± 25	>2000	−	1250 ± 750	normal
267040	125 ± 75	150 ± 50	63 ± 38	−	−	500 ± 500	normal
231018	300 ± 200	300 ± 200	175 ± 75	−	−	−	no MT binding
naphthalene sulfonates							
267154	5 ± 5	6.3 ± 3.8	2.5 ± 2.5	>2000	30 ± 10	>1000	no MT binding
267009	12.5 ± 7.5	12.5 ± 7.5	12.5 ± 7.5	>2000	>40	500 ± 500	no MT binding
266324	125 ± 75	125 ± 75	50 ± 50	>2000	>100	1250 ± 750	no MT binding
195710	150 ± 50	150 ± 50	−	>2000	−	−	no MTs
230702	550 ± 450	300 ± 200	125 ± 125	>1000	−	−	no MT binding
miscellaneous							
17488	125 ± 75	125 ± 75	25 ± 25	>2000	−	>1000	normal
128813	125 ± 75	63 ± 38	−	>2000	−	1250 ± 750	normal
184739	550 ± 450	625 ± 375	125 ± 125	−	−	−	normal

[a] The mean inhibitory concentration (IC_{50}) of a compound is contained in the interval $[A + (B - A)/2] \pm [(B - A)/2]$, where no inhibition is observed with the compound at concentration A μM and complete inhibition is observed at concentration B μM (for details, see Methods). [b] K560-MT and [c]ncd-MT denote microtubule-stimulated kinesin and ncd ATPase, respectively. [d]unc104 is another kinesin superfamily member. [e] BAS is the basal ATPase rate in the absence of microtubules. [f]ATPase of actin-activated myosin II. The double asterisks (**) indicate that an activation of the basal hydrolysis rate was observed (see Results). [g]1 mM compound prevented microtubules from binding kinesin (no MT binding) in an in vitro microtubule-gliding assay, showed normal motility (normal), or disrupted microtubule stability (no MTs).

the number of inhibitors within each structural class.

To identify the strongest binding compounds, we assayed the 22 submillimolar inhibitors at diluted levels until control ATPase was recovered. These serial dilutions were designed to give estimates of the compounds' IC_{50} values (see Methods). Of the 22 submillimolar compounds, 13 showed inhibition of K560's microtubule-stimulated ATPase no lower than 100 μM (Table 1, column K560-MT). Of these, eight compounds continued to block hydrolysis below 50 μM. The strongest three inhibitors were compounds RBL, 11663, and 267154, inhibiting K560-MT between 1 and 10 μM (Table 1).

To examine the selectivity of these compounds, serial dilutions were also performed using other kinesin superfamily members. We expected our kinesin inhibitors to have similar activity against ncd because of the similarity of the docking sites between the two motors. Consistent with this hypothesis, the differences in activity between K560 and ncd were small. Notably, however, compounds RBL, 1617, and 1624 were stronger inhibitors of ncd-MT activity than of K560-MT activity (Table 1), while compound 1613 was a weaker ncd-MT inhibitor. The highest selectivity was the 2−5-fold potency difference exhibited by compounds RBL (stronger against ncd-MT) and 1613 (stronger against K560-MT). We also tested for inhibition and selectivity against yet a third kinesin, unc104. Compounds RBL, 1617, 19164, and 17488 were stronger inhibitors of unc104-MT than of K560-MT. Compounds 22269, 1613, and 267040 were stronger inhibitors of unc104-MT than of ncd-MT. Thus, the submillimolar inhibitors exhibited a range of micromolar inhibition against kinesin ATPase, with the more potent compounds showing a 2−5-fold range of selectivity for superfamily members. To examine the specificity of these compounds outside the kinesin superfamily, we also measured the inhibition of actin-stimulated ATPase of myosin (Table 1). Compound RBL was only slightly less potent against actomyosin than kinesin, with inhibition around 25 μM, but compounds 1613 and 46964 exhibited 10−40-fold specificity.

We also tested for inhibition in the absence of microtubules. The basal hydrolysis in kinesin is about 1000 times slower than that stimulated by microtubules. Compounds that did not inhibit basal ATPase and did inhibit microtubule-stimulated ATPase were likely candidates for inhibition by microtubule binding and/or disruption. With the exception of RBL, all of the compounds we tested did not inhibit the basal ATPase of K560. This combination of results raised the possibility that these compounds were actually inhibiting ATPase via microtubule binding and/or destabilization and not via kinesin binding. However, we found some of these compounds (RBL, 5044, 267154) did inhibit ncd's basal hydrolysis below 100 μM, indicating an inhibitory mechanism involving kinesin binding and not purely microtubule-related effects. In any case, these results suggested a much larger selectivity against the basal hydrolysis than against that stimulated by microtubules. In the case of compound 267154, this specificity is at least 60-fold.

It is likely that compounds binding to kinesin could actually stimulate the basal ATPase rate. This effect was reported for AS-2, which inhibited microtubule-stimulated ATPase, yet increased the basal hydrolysis rate by up to 3-fold (*13*). Likewise, we found that compound 11663 activated the basal ATPase (250% of control) at 50 μM.

Compound RBL showed a smaller degree of basal rate activation (124% of control) at 10 μM, but by 40 μM, the basal rate was completely inhibited. It should be noted, however, that the basal rate activation effects of these two compounds were not observed for ncd: compound RBL inhibited ncd's basal hydrolysis (Table 1), and compound 11663 did not inhibit hydrolysis at 50 μM. In summary, we found greater variability between the kinesin families in the compounds' effect on kinesin basal ATPase rates than on the microtubule-stimulated rates.

Many of the compounds found to inhibit kinesin ATPase also interrupt kinesin's activity in an in vitro microtubule-gliding assay (Table 1). In this assay, K560 is bound to the coverslip surface, and microtubules are observed to bind to this kinesin and move. The concentration of kinesin was diluted to a point 10-fold above the concentration at which no microtubules bind (0.02−0.2 μg/mL). At this surface density of K560, many compounds prevented microtubules from binding to the surface (Table 1). However, these same compounds had no observable effect on microtubule binding and velocity when measured at significantly higher concentrations of kinesin (0.2−2 μg/mL, data not shown), consistent with the microtubule-competitive nature of these inhibitors. At least one compound was found to interfere with kinesin ATPase by disrupting microtubule stability (compound 195710, Table 1).

Inhibition by Rose Bengal Lactone. We focused on rose bengal lactone (RBL), one of the more potent inhibitors of kinesin, to further characterize its mechanism of inhibition. Understanding RBL's mode of kinesin inhibion could be exploited in future ligand design efforts. First we wished to address whether RBL competes with microtubules or with ATP for binding kinesin. Steady-state kinetic experiments revealed RBL's inhibition to be competitive with microtubules but not with ATP. Figure 4A shows that at 1 μM microtubules, 5 μM RBL partially inhibited K560 ATPase, while excess microtubules removed this inhibition. On the other hand, excess ATP did not reduce RBL's inhibition (Figure 4B). Thus, RBL interfered with microtubule binding and not ATP binding. In fact, RBL prevented kinesin from cosedimenting with microtubules in the presence of a nonhydrolyzable ATP analogue, AMP-PMP (Figure 5), further implicating a microtubule-competitive mechanism of inhibition.

The fluorescence of RBL provided a convenient spectroscopic signal to monitor the binding of RBL to kinesin. We expected a reduction in the lifetime-averaged rotational diffusion of RBL upon binding kinesin. Accordingly, the steady-state anisotropy of RBL was 0.232 and increased to 0.347 upon binding to kinesin (Figure 6). The increase in steady-state anisotropy upon binding suggests that RBL reduced its rotational correlation time by associating with the much larger kinesin. Using the anisotropy signal to calculate the amount of free (unbound) RBL, a binding curve with a dissociation constant of 2.4 μM was determined (see Figure 6).

RBL's Binding Site. We decided to test whether RBL, a large hydrophobic molecule, was nonspecifically associating with kinesin. There is considerable precedent for large organic dyes binding to hydrophobic surfaces of proteins (*38*−*40*), especially on hydrophobic regions exposed by proteins undergoing conformational changes (*41*−*44*). However, the RBL dissociation constant and inhibition levels, in the low micromolar range, suggested a more specific mode of association than is typical of nonspecific organic dyes on proteins. This encouraged the pursuit of a structural description of RBL binding.

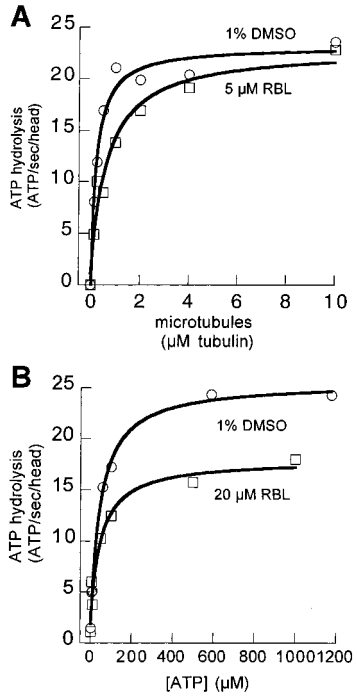

FIGURE 4: (A) Effect of 5 μM RBL (squares) on ATPase, shown plotted against microtubule concentration, and compared to a DMSO control (circles). (B) Effect of 20 μM RBL (squares) on ATPase, shown plotted against ATP concentration (with 7 μM microtubules), and compared to a DMSO control (circles). ATPase was measured according to the coupled enzyme assay (see Methods). A Michaelis−Menten model was fit to the data by nonlinear regression (lines). Kinesin's apparent Michaelis constant (K_m) for microtubules increased ~10-fold in the presence of 5 μM RBL (squares, panel A); 20 μM RBL (squares, panel B) reduced the control (circles, panel B) V_{max} 65% with no change in kinesin's K_m for ATP.

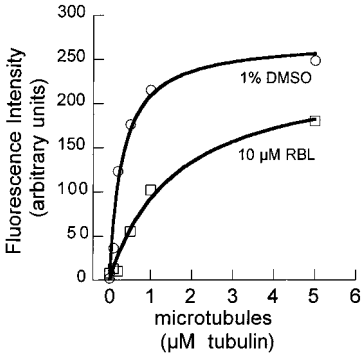

FIGURE 5: RBL reduced the binding of kinesin to microtubules in the presence of the nonhydrolyzable analogue AMP-PNP. The amount of kinesin cosedimented in a pellet of microtubules was measured by the fluorescence of GFP fused to kinesin (see Methods) in the presence (squares) and absence (circles) of RBL. The intensity of fluorescence (I) as a function of microtubule concentration, [MT], was fit by nonlinear regression according to the equation: $I = I_o[MT]/(K_{dapp} + [MT])$, where I_o is an estimate of the limiting intensity at saturating [MT] and K_{dapp} is kinesin's apparent microtubule dissociation constant. 10 μM RBL did not change I_o, related to the amount of microtubule-bound kinesin at saturating [MT], but did cause a ~5-fold increase in K_{dapp} from 0.3 to 1.6 μM.

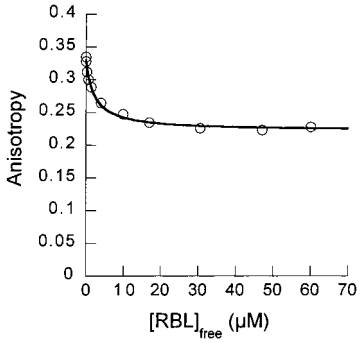

FIGURE 6: Binding of RBL to kinesin as measured by its steady-state fluorescence anisotropy. Increasing concentrations of RBL in DMSO were added to a cuvette containing a fixed amount of K560 (2 μM), buffer, and DMSO (6.7%). The anisotropy values (A), as a function of unbound RBL ($[RBL]_{free}$), were fit according to the equation: $A = (A_\infty - A_0)[RBL]_{free}/(K_d + [RBL]_{free}) + A_\infty$. The anisotropy of completely unbound RBL (A_∞, asymptote) was 0.232, and the anisotropy of completely bound RBL (A_0, intercept) was 0.347. These values were then used to calculate the fraction of unbound ($[RBL]_{free}$) of the total amount of added RBL at each measured anisotropy. The anisotropy values were then plotted against this calculated $[RBL]_{free}$, and fitting the above equation yielded the dissociation constant (K_d) of 2.4 μM.

We used fluorescence resonance energy transfer (FRET) to independently measure five distances, each between a FRET donor-labeled position in the motor domain and a kinesin-bound RBL, the FRET acceptor. Figure 1 shows these donor positions in stereo. At each position, a surface-exposed cysteine residue was covalently labeled with the donor fluorophore 7-diethylamino-3-(4′-maleimidylphenyl)-4-methylcoumarin (CPM). A total of five monomeric, single surface-exposed cysteine constructs (cysteine-light mutants, CLM) were labeled in turn: CLM-C330, CLM-C220, CLM-C28, CLM-C149, and CLM-C103. The ATPase of the CPM-labeled kinesin was inhibited by RBL, and anisotropy measurements showed RBL binding at 1.5 μM (data not shown).

In a typical experiment, CPM fluorescence (excitation 395 nm, and 470 nm peak emission) was measured for a CPM-labeled kinesin (5 μM) with 0−33 μM RBL. For all CPM-labeled kinesins, the intensities dropped as a function of RBL concentration, indicating that RBL was binding to kinesin. The intensity drop was saturated by 33 μM added RBL, and the addition of the denaturant guanidinium chloride removed this effect. At this saturating intensity, each donor-labeled kinesin had a bound acceptor RBL, thus yielding the FRET efficiencies and resulting distances reported in Table 2.

All five FRET distances were used to uniquely locate the RBL binding site in kinesin's three-dimensional structure. Five spheres were centered at each donor position and given a radius according to their FRET distance. After allowing for an error of ±4 Å in the radii, the intersection of the five spheres defined a volume that contained the bound RBL in its docked L8/β5 site. The intersection of spheres, describing an allowed binding region for RBL, was constrained to such an extent that only three complete residues, in addition to the docked RBL, were contained inside: Tyr 164, Pro 163, and Val 162. Figure 7 shows a stereo diagram of bound RBL. In summary, the volume contained at least one atom from the residues between Asp 156 and Val 165 on one side of the pocket, and various atoms from Glu 170 and Lys 213 on the other side. When we allowed for more error in the FRET distances, the size of the allowed binding region increased but still contained our docked RBL at its center. The multiple donor positions do not produce any internal inconsistencies, adding confidence to this location. Our method of locating of RBL's binding site makes an assumption that the structure of the donor-labeled CLM kinesin is not altered dramatically from the crystal structure. This assumption is justified from the various crystal structures of kinesin solved to date that show remarkably similar three-dimensional structures despite altered amino acid sequences. Furthermore, fluorescent and paramagnetic probes labeling some of these same cysteines showed normal ATP hydrolysis rates and motility (S. Rice, personal communication). Thus, these FRET measurements indicate specific binding of RBL at the L8/β5 site.

Table 2: FRET Transfer Efficiencies with RBL Bound to Kinesins with Different Positions of Coumarin Donor[a]

donor position	transfer efficiency[b] (%)	X-tal distance[c] (Å)	FRET distance[d] (Å)
CLM-C330	100	16	<22
CLM-C220	100	21	<22
CLM-C149	100	21	<22
CLM-C103	85	33	34
CLM-C28	51	47	45

[a] Donor fluorophore CPM was covalently attached to single surface-exposed cysteines engineered at the numbered positions shown in Figure 1. [b] Efficiencies are expressed using saturating acceptor intensities from the limiting asymptote of a binding curve fit to the decay in intensity as a function of total added RBL (see Methods). [c] X-tal distances expressed as the distance between the carbon atom para to the oxygen atom in the central ring of RBL (Figure 3) and the Cα carbon at the numbered position in the human crystal structure (Protein Data Bank entry 1bg2), where position 330 is measured using the dimeric structure from rat (Protein Data Bank entry 2kin). [d] FRET distance is the calculated distance using $R_o = 45$ Å. At this R_o, all FRET distances less than 22 Å correspond to efficiencies more than 99%.

DISCUSSION

DOCK Screening for Inhibitors. The structure-based computer screening described here proved to be a rapid method to identify submillimolar kinesin inhibitors. The only other known kinesin inhibitor (AS-2) was identified in a biochemical screen of marine sponge extracts (*13*). The IC_{50} of AS-2 (2.7 μM) is comparable to the best inhibitors found by our computer screen, and its potency among other superfamily members was within a 5-fold difference, comparable to the selectivity of several compounds in Table 1.

The inhibitors presented in our study are similar to selective anthraquinone-, phenolphthalein-, and fluorescein-based inhibitors presented in other structure-based computer screening studies of other enzyme systems (*15*, *45*, *46*). The inhibitors in Table 1 contain common cores of various known enzyme inhibitors and drugs. For example, compounds containing the anthraquinone ring system are common antitumor drugs, and have been reported to inhibit other nucleotide-requiring systems such as Ser/Thr kinases (*47*), xanthine oxidase (*48*), and DHFR (*45*), and have been reported elements of naturally occurring antibiotics (*49*). With a more systematic combinatorial approach, it is possible that further permutations on the structural cores in Figure 3 may produce more specific and tighter binding kinesin inhibitors.

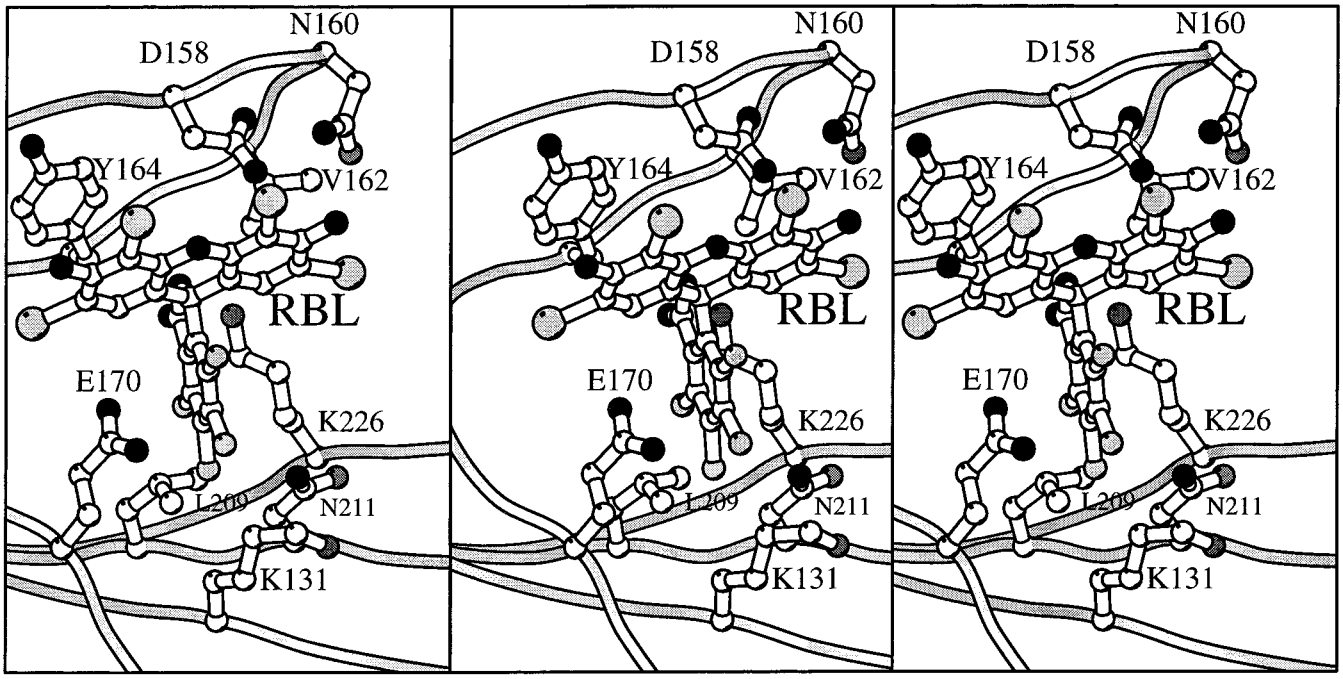

FIGURE 7: Stereo diagram of RBL's docked orientation. This docked location was confirmed by independent FRET measurements (see text). Residues with atoms closest to RBL are shown in figure. The central core's β-sheet contains the residues K226, L209, N211, and K131 shown in figure. Loop 8 and strand β5 contain the residues D158, N160, V162, Y164, and E170 shown in figure. See Figure 1 for secondary structural elements and location of the L8/β5 binding site. Oxygen atoms are black, nitrogen gray, and carbon white. See Figure 3 for the two-dimensional structure of RBL. Cross-eyed view is in left two images; wide-eyed view is in right two images. Figure made with MolScript (*50*).

Our structure-based approach did not include tests for inhibition in vivo. One approach would be to look for a lethality during mitotic division, which could occur via an inhibitory action against kinesins. Some of the large charged compounds, however, may not traverse the cell membrane and would require injection, as was necessary to demonstrate AS-2 lethality in early *Drosophila* embryos (*13*). In many cases, however, it would be uncertain whether the observed effects of these compounds after injection would be a result of kinesin inhibition or other effects, such as inhibition of other enzymes, binding to DNA or other proteins, microtubule destabilization, or even free radical production. While many of our inhibitors could indeed bind to other protein systems, their inhibition of kinesin in vitro made them especially relevant, considering there is only one other reported inhibitor. The microtubule-competitive nature of these inhibitors suggested binding away from the active site, and thus centered our efforts on using RBL to characterize a novel binding pocket for kinesin inhibition.

RBL Inhibition. Historically, the search for enzyme inhibitors has been more successful at discovering molecules that compete for binding at the active site, while inhibitors interfering with protein−protein association distal to the active site have been more difficult to discover. In this study we discovered a compound, RBL, capable of disrupting the interaction between kinesin and microtubules. Biochemically, RBL was shown to reduce kinesin's affinity for microtubules and not interfere with kinesin's affinity for ATP. This result implicated RBL's inhibition to occur via binding at a site involved in microtubule stimulation. Since RBL also reduced the affinity of kinesin's strongly bound, AMP-PNP state for microtubules, we concluded that RBL competed with microtubule binding.

Structurally, we used information in the crystallographic model to localize RBL's binding site to the L8/β5 pocket. The measured binding site of RBL happened to correspond with the original docked position. It is important to point out that we did not dock compounds at all possible binding sites on kinesin, and discovering that RBL bound at the docked site served to validate this pocket as a target for structure-based inhibitor design. Initially, this pocket was chosen mainly due to its recessed topology, suitable for our scoring functions, which only considered ligand−protein interactions, not interactions between ligand and solvent. The FRET experiments we used here to identify the ligand binding site were as an alternative to crystallographic confirmation, and are the first docking study to use structural information from FRET.

The RBL binding site is likely to be important for the hypothesized conformational changes during kinesin motility. This study confirms the microtubule binding role of loop 8, as was suggested by proteolytic mapping of the kinesin−microtubule interface (*37*) and alanine-scanning mutagenesis (*32*) of this face of the protein. Furthermore, our results suggest that the L8/β5 binding pocket is an important surface feature contributing to kinesin's nucleotide-dependent affinity for microtubules, and validates the structure-based design of ligands at this pocket. With the increasing number of kinesin structures being solved, future work will be directed toward the design of inhibitors with tighter and more selective inhibition among the kinesin motors.

NOTE ADDED IN PROOF

The paper describing the properties of the labeled cysteine mutants of kinesin has been published (*51*).

ACKNOWLEDGMENT

Ryan Case, Kurt Thorn, Dan Pierce, and Roger Cooke generously provided the motors ncd-GFP, K560-GFP, unc104, and myosin II, respectively. We thank Cindy Hart for help purifying, expressing K560, and cloning CLM349, and Sarah Rice for help labeling CLM349. We also thank the UCSF Computer Graphics Laboratory (T. Ferrin, Director).

REFERENCES

1. Vale, R. D., and Fletterick, R. J. (1997) *Annu. Rev. Cell Dev. Biol. 13*, 745−777.
2. Kull, F. J., Sablin, E. P., Lau, R., Fletterick, R. J., and Vale, R. D. (1996) *Nature 380*, 550−555.
3. Sack, S., Muller, J., Marx, A., Thormahlen, M., Mandelkow, E. M., Brady, S. T., and Mandelkow, E. (1997) *Biochemistry 36*, 16155−16165.
4. Kozielski, F., Sack, S., Marx, A., Thormahlen, M., Schonbrunn, E., Biou, V., Thompson, A., Mandelkow, E.-M., and Mandelkow, E. (1997) *Cell 91*, 985−994.
5. Sablin, E. P., Kull, F. J., Cooke, R., Vale, R. D., and Fletterick, R. J. (1996) *Nature 380*, 555−559.
6. Sablin, E. P., Case, R. B., Dai, S. C., Hart, C. L., Ruby, A., Vale, R. D., and Fletterick, R. J. (1998) *Nature 395*, 813−816.
7. Gulick, A. M., Song, H., Endow, S. A., and Rayment, I. (1998) *Biochemistry 37*, 1769−1777.
8. Rayment, I., Rypniewski, W. R., Schmidt-Base, K., Smith, R., Tomchick, D. R., Benning, M. M., Winkelmann, D. A., Wesenberg, G., and Holden, H. M. (1993) *Science 261*, 50−58.
9. Vale, R. D. (1996) *J. Cell Biol. 135*, 291−302.
10. Kull, F. J., Vale, R. D., and Fletterick, R. J. (1998) *J. Muscle Res. Cell Motil. 19*, 877−886.
11. Hamel, E. (1996) *Med. Res. Rev. 16*, 207−231.
12. Rowinsky, E. K., and Donehower, R. C. (1991) *Pharmacol. Ther. 52*, 35−84.
13. Sakowicz, R., Berdelis, M. S., Ray, K., Blackburn, C. L., Hopmann, C., Faulkner, D. J., and Goldstein, L. S. (1998) *Science 280*, 292−295.
14. Rutenber, E., Fauman, E. B., Keenan, R. J., Fong, S., Furth, P. S., Ortiz de Montellano, P. R., Meng, E., Kuntz, I. D., DeCamp, D. L., Salto, R., Rose, J. R., Craik, C. S., and Stroud, R. M. (1993) *J. Biol. Chem. 268*, 15343−15346.
15. Shoichet, B. K., Stroud, R. M., Santi, D. V., Kuntz, I. D., and Perry, K. M. (1993) *Science 259*, 1445−1450.
16. Bodian, D. L., Yamasaki, R. B., Buswell, R. L., Stearns, J. F., White, J. M., and Kuntz, I. D. (1993) *Biochemistry 32*, 2967−2978.
17. Somoza, J. R., Skillman, A. G., Munagala, N. R., Oshiro, C. M., Knegtel, R. M. A., Mpoke, S., Fletterick, R. J., Kuntz, I. D., and Wang, C. C. (1998) *Biochemistry 37*, 5344−5348.
18. Kuntz, I. D. (1992) *Science 257*, 1078−1082.
19. Kuntz, I. D., Blaney, J. M., Oatley, S. J., Langridge, R., and Ferrin, T. E. (1982) *J. Mol. Biol. 161*, 269−288.
20. Meng, E. C., Shoichet, B. K., and Kuntz, I. D. (1992) *J. Comput. Chem. 13*, 505−524.
21. Ewing, T. J. A., and Kuntz, I. D. (1997) *J. Comput. Chem. 18*, 1175−1189.
22. Pearlman, R. S. (1998) in *CONCORD User's Manual*, distributed by Tripos Inc., St. Louis, MO.
23. Pearlman, R. S. (1987) *Chem. Des. Auto. News 2*, 1.
24. Nicholls, A., Sharp, K., and Honig, B. (1991) *Proteins: Struct., Funct., Genet. 11*, 281−296.
25. Skillman, A. G. (1999) Ph.D. Thesis, University of California, San Francisco.
26. *Daylight, Version 4.61* (1997) Daylight Chemical Information Systems, Inc., Santa Fe, NM.
27. Ferrin, T. E., and Huang, C. C. (1988) *J. Mol. Graphics 6*, 13−27, 36−37.
28. Ferrin, T. E., Couch, G. S., and Huang, C. C. (1991) *J. Mol. Graphics 9*, 27−32, 37−38.
29. *SYBYL, 6.5* (1998) Tripos Inc., St. Louis, MO.
30. Hyman, A., Dreschel, D., Kellogg, D., Salser, S., Sawin, K., Steffen, P., Wordeman, L., and Mitchison, T. (1990) *Methods Enzymol. 196*, 303−319.
31. Geladopoulos, T. P., Sotiroudis, T. G., and Evangelopoulos, A. E. (1991) *Anal. Biochem. 192*, 112−116.
32. Woehlke, G., Ruby, A. K., Hart, C. L., Ly, B., Hom-Booher, N., and Vale, R. D. (1997) *Cell 90*, 207−216.
33. Huang, T. G., Suhan, J., and Hackney, D. D. (1994) *J. Biol. Chem. 269*, 16502−16507.
34. Griffin, B. A., Adams, S. R., and Tsien, R. Y. (1988) *Science 281*, 269−272.
35. dos Remedios, C. G., and Moens, P. D. (1995) *J. Struct. Biol. 115*, 175−185.
36. Van Der Meer, B. W., Coker, G., and Chen, S.-Y. S. (1994) in *Resonance Energy Transfer. Theory and Data*, VCH, Inc., New York.
37. Alonso, M. C., van Damme, J., Vandekerckhove, J., and Cross, R. A. (1998) *EMBO J. 17*, 945−951.
38. Stryer, L. (1968) *Science 162*, 526−533.
39. Brand, L., and Gohlke, J. R. (1972) *Annu. Rev. Biochem. 41*, 843−868.
40. Edmundson, A. B., Ely, K. R., and Herron, J. N. (1984) *Mol. Immunol. 21*, 561−576.
41. Cheung, H. C., and Morales, M. F. (1969) *Biochemistry 8*, 2177−2182.
42. Borejdo, J. (1983) *Biochemistry 22*, 1182−1187.
43. Daban, J. R., and Guasch, M. D. (1980) *Biochim. Biophys. Acta 625*, 237−247.
44. Semisotnov, G. V., Rodionova, N. A., Razgulyaev, O. I., Uversky, V. N., Gripas, A. F., and Gilmanshin, R. I. (1991) *Biopolymers 31*, 119−128.
45. Gschwend, D. A., Sirawaraporn, W., Santi, D. V., and Kuntz, I. D. (1997) *Proteins: Struct., Funct., Genet. 29*, 59−67.
46. Hoffman, L. R., Kuntz, I. D., and White, J. M. (1997) *J. Virol. 71*, 8808−8820.
47. Yim, H., Lee, Y. H., Lee, C. H., and Lee, S. K. (1999) *Plant. Med. 65*, 9−13.
48. Sheu, S. Y., and Chiang, G. C. (1997) *Anticancer Res. 17*, 3293−3296.
49. Goto, M., Masegi, M., Yamauchi, T., Chiba, K., Kuboi, Y., Harada, K., and Naruse, N. (1998) *J. Antibiot. 51*, 539−544.
50. Kraulis, P. J. (1991) *J. Appl. Crystallogr. 24*, 946−950.
51. Rice, S., Lin, A. W., Safer, D., Hart, C. L., Naber, N., Carragher, B. O., Cain, S. M., Pechatnikova, E., Wilson-Kubalek, E. M., Whittaker, M., Pate, E., Cooke, R., Taylor, E. W., Milligan, R. A., and Vale, R. D. (1999) *Nature 402*, 778−784.

BI992474K